

1 **Temporal characteristics of atmospheric ammonia and nitrogen dioxide over China based on**
2 **emission data, satellite observations and atmospheric transport modeling since 1980**

3 Lei Liu ^a, Xiuying Zhang ^{a,*}, Wen Xu ^b, Xuejun Liu ^b, Yi Li ^c, Xuehe Lu ^a, Yuehan Zhang ^d, Wuting
4 Zhang ^{a,e}

5 ^a Jiangsu Provincial Key Laboratory of Geographic Information Science and Technology, International
6 Institute for Earth System Science, Nanjing University, Nanjing 210023, China

7 ^b College of Resources and Environmental Sciences, Centre for Resources, Environment and Food
8 Security, Key Lab of Plant-Soil Interactions of MOE, China Agricultural University, Beijing 100193,
9 China

10 ^c Air Quality Division, Arizona Department of Environmental Quality, Phoenix, AZ, 85007, USA

11 ^d School of Atmospheric Sciences, Nanjing University, Nanjing, China

12 ^e Jiangsu Center for Collaborative Innovation in Geographical Information Resource Development and
13 Application, Nanjing 210023, China

14 * Corresponding authors: Xiuying Zhang (lzhxy77@163.com)

15 **Abstract**

16 China is experiencing intense air pollution caused in large part by anthropogenic emissions of reactive
17 nitrogen (Nr). Atmospheric ammonia (NH₃) and nitrogen dioxide (NO₂) are the most important
18 precursors for Nr compounds (including N₂O₅, HNO₃, HONO and particulate NO₃⁻ and NH₄⁺) in the
19 atmosphere. Understanding the changes of NH₃ and NO₂ has important implications for the regulation
20 of anthropogenic Nr emissions, and is a requirement for assessing the consequence of environmental
21 impacts. We conducted the temporal trend analysis of atmospheric NH₃ and NO₂ on a national scale

22 since 1980 based on emission data (during 1980-2010), satellite observations (for NH₃ since 2008 and
23 for NO₂ since 2005) and atmospheric chemistry transport modeling (during 2008-2015).

24 Based on the emission data, during 1980-2010, both significant continuous increasing trend of NH₃ and
25 NO_x were observed from REAS (Regional Emission inventory in Asia, for NH₃ 0.17 kg N ha⁻¹ y⁻² and
26 for NO_x 0.16 kg N ha⁻¹ y⁻²) and EDGAR (Emissions Database for Global Atmospheric Research, for
27 NH₃ 0.24 kg N ha⁻¹ y⁻² and for NO_x 0.17 kg N ha⁻¹ y⁻²) over China. Based on the satellite data and
28 atmospheric chemistry transport modeling named as the Model for Ozone and Related chemical
29 Tracers, version 4 (MOZART-4), the NO₂ columns over China increased significantly from 2005 to
30 2011 and then decreased significantly from 2011 to 2015; the satellite-retrieved NH₃ columns from
31 2008 to 2014 increased at a rate of 2.37% y⁻¹. The decrease in NO₂ columns since 2011 may result from
32 more stringent strategies taken to control NO_x emissions during the 12th Five-Year-Plan, while no
33 control policy focused on NH₃ emissions. Our findings provided an overall insight on the temporal
34 trends of both NO₂ and NH₃ since 1980 based on emission data, satellite observations and atmospheric
35 transport modeling. These findings can provide a scientific background for policy-makers that are
36 attempting to control atmospheric pollution in China. Moreover, the multiple datasets used in this study
37 have implications for estimating long-term Nr deposition datasets to assess its impact on soil, forest,
38 water and greenhouse balance.

39 **Keywords:** trends, seasonal cycle, ammonia

40 **1. Introduction**

41 Reactive nitrogen (Nr) emissions have increased significantly in China due to anthropogenic activities
42 such as increased combustion of fossil fuels, over-fertilization and high stocking rates of farm animals
43 (Canfield et al., 2010;Galloway et al., 2008;Liu et al., 2013). Elevated Nr in the environment has led to

44 a series of effects on climate change and ecosystems, e.g. biodiversity loss, stratospheric ozone
45 depletion, air pollution, freshwater eutrophication, the potential alteration of global temperature,
46 drinking water contamination, dead zones in coastal ecosystems and grassland seed bank depletion
47 (Basto et al., 2015;Lan et al., 2015;Shi et al., 2015). Atmospheric reactive N emissions are dominated
48 by nitrogen oxides ($\text{NO}_x = \text{NO} + \text{NO}_2$) and ammonia (NH_3) (Li et al., 2016a;Galloway et al., 2004).
49 Atmospheric NO_2 and NH_3 are the most important precursors for Nr compounds including N_2O_5 , HNO_3 ,
50 HONO and particulate NO_3^- and NH_4^+ in the atmosphere (Xu et al., 2015;Pan et al., 2012). Therefore,
51 an understanding of both the spatial and temporal patterns of NO_2 and NH_3 is essential for evaluating
52 N-enriched environmental effects, and can provide the scientific background for N pollution mitigation.
53 To investigate the spatial and temporal variations of atmospheric NO_2 and NH_3 , ground measurements
54 are acknowledged to be an effective way in monitoring the accurate concentrations of NO_2 and NH_3
55 (Xu et al., 2015;Pan et al., 2012;Meng et al., 2010). Ground measurements of NO_2 concentrations in
56 China, including about 500 stations in 74 cities, have been monitored and reported to the public since
57 January 2013 (Xie et al., 2015). By the end of 2013, this network was extended with hourly NO_2
58 concentrations from more than 850 stations in 161 cities. However, there are fewer NH_3 measurements
59 across China than NO_2 measurements. The China Agricultural University has organized a Nationwide
60 Nitrogen Deposition Monitoring Network (NNDMN) since 2010, consisting of 43 monitoring sites
61 covering urban, rural (cropland) and background (coastal, forest and grassland) areas across China (Xu
62 et al., 2015;Liu et al., 2011). Xu et al. (2015) reported the ground NH_3 concentrations throughout China
63 for the first time, providing great potential to understand the ground NH_3 concentrations on a national
64 scale. Other networks include (1) the Chinese Ecosystem Research Network (CERN) which was
65 established in 1988, including 40 field stations (Fu et al., 2010). However, to our knowledge, there are

66 no detailed reports about ground NH₃ concentrations from CERN on a national scale. (2) Four Chinese
67 cities (Xiamen, Xi-An, Chongqing and Zhuhai) have joined the Acid Deposition Monitoring Network
68 in East Asia (EANET) since 1999. However, only one site (Hongwen, Xiamen) in EANET measured
69 the ground NH₃ concentrations and that data is not continuous. Finally, ground NH₃ concentrations at
70 ten sites in Northern China from 2007 to 2010 have been reported by Pan et al. (2013). All of the above
71 ground measurements provide the potential to understand NH₃ and NO₂ concentrations on a regional
72 scale. However, there is limited information on the spatial and temporal variations of NH₃ and NO₂ in
73 the atmosphere across China. This is due to the limited observation sites and monitoring period, as well
74 as given the uneven distribution of the monitoring sites. Importantly, atmospheric NH₃ and NO₂
75 monitoring based on ground-based local sites may have limited spatial representativeness of the
76 regional scale as both NH₃ and NO₂ are highly variable in time and space (Clarisse et al., 2009; Wichink
77 Kruit et al., 2012; Boersma et al., 2007).

78 In order to complement ground-based measurements, satellite observation of NH₃ and NO₂ is a
79 welcome addition for analyzing the recent trends of NH₃ and NO₂ in the atmosphere. Satellite remote
80 sensing offers an opportunity to monitor atmospheric NH₃ and NO₂ with high temporal and spatial
81 resolutions (Warner et al., 2017; Li et al., 2016b). NO₂ was measured by multiple space-based
82 instruments including the Global Ozone Monitoring Experiment (GOME), SCanning Imaging
83 Absorption SpectroMeter for Atmospheric CHartography (SCIAMACHY), Ozone Monitoring
84 Instrument (OMI) and Global Ozone Monitoring Experiment-2 (GOME-2). The OMI NO₂ provides the
85 best horizontal resolution ($13 \times 24 \text{ km}^2$) among instruments in its class and near-global daily coverage
86 (Levelt et al., 2007). OMI observations have been widely applied in environmental-related studies and
87 for the support of emission control policy (Russell et al., 2012; Zhao and Wang, 2009; Castellanos et al.,

88 2015;Lamsal et al., 2015;Liu et al., 2016a;Foy et al., 2016). First measurements of NH₃ from space
89 were reported over Beijing and San Diego areas with the Tropospheric Emission Spectrometer (TES)
90 (Beer et al., 2008) and in fire plumes in Greece with the Infrared Atmospheric Sounding Interferometer
91 (IASI) (Coheur et al., 2009). The first global map of NH₃ was created from IASI measurements by
92 correlating the observed brightness temperature differences to NH₃ columns using the averaged
93 datasets in 2008 (Clarisse et al., 2009). Shortly after that, many studies focused on developing
94 techniques to gain more reliable NH₃ columns (Whitburn et al., 2016a;Van Damme et al., 2014b),
95 validating the retrieved NH₃ columns using the ground measurements (Van Damme et al.,
96 2014a;Dammers et al., 2016) and comparing the data with the results of the atmospheric chemistry
97 transport models (Van Damme et al., 2014c;Whitburn et al., 2016a), and the estimated NH₃ columns
98 obtained from Fourier transform infrared spectroscopy (FTIR) (Dammers et al., 2016). The retrieval
99 algorithm of obtaining IASI NH₃ columns was based on the method described in Whitburn et al. (2016).
100 Two main steps were performed to derive the NH₃ columns from the satellite measurements. First,
101 derive the spectral hyperspectral range index (HRI) based on each IASI observations (Walker et al.,
102 2011;Van Damme et al., 2014b). Second, convert HRI to NH₃ columns based on a constructed neural
103 network with input parameters including vertical NH₃ profile, satellite viewing angle, surface
104 temperature and so on (Whitburn et al., 2016a). The progresses made on the satellite techniques
105 provide possibility for understanding both the spatial and temporal variations of NH₃ and NO₂ in the
106 atmosphere.

107 In addition to satellite observations, the emission data are also very important for investigating the
108 temporal trends of NH₃ and NO₂ such as the IIASA inventory (Cofala et al., 2007), EDGAR (Emission
109 Database for Global Atmospheric Research, RAINS-Asia (Regional Air Pollution Information and

110 Simulation) and Asia REAS (Regional Emission inventory in Asia). REAS is considered as the first
111 inventory by integrating historical, current and future emissions data for Asia based on a consistent
112 methodology (Ohara et al., 2007), and EDGAR is the global emission data with 0.1 by 0.1 grid, which
113 has the highest spatial resolution among different datasets mentioned above. Thus, REAS and EDGAR
114 are used to analyze the historical trends of NH₃ and NO₂ during 1980-2010 in this study. Based on the
115 EDGAR emission data, a widely used atmospheric transport model named as the Model for Ozone and
116 Related chemical Tracers, version 4 (MOZART-4) was also used to model the temporal trend of NH₃
117 and NO₂ columns during 2008-2015 in comparison with the temporal trends of NH₃ and NO₂ columns
118 measured by satellite instruments.

119 We aim at getting an overall insight on the temporal trends of both NO₂ and NH₃ since 1980 based on
120 the multiple datasets including the emission data, satellite observations and atmospheric transport
121 modeling. We herein show the Chinese national trend of REAS and EDGAR NH₃ and NO_x emission
122 data during 1980-2010, satellite-retrieved NH₃ during 2008-2015 and NO₂ columns (2005-2015), and
123 atmospheric transport chemistry modeling NH₃ and NO₂ columns (2008-2015). It should be noted here
124 that the satellite NH₃ columns were retrieved from the IASI, and can only be obtained since 2008. It is
125 beneficial to analyze the temporal variations of both NH₃ and NO₂, hence providing a scientific basis
126 for policy makers to reduce N-enriched environmental pollution in China.

127 **2. Materials and methods**

128 **2.1. NH₃ and NO₂ Emissions**

129 We examined the emission inventory dataset for Asia REAS (Regional Emission inventory in Asia)
130 with 0.5°×0.5° resolution for the period 1980-2010, and analyzed the temporal trends of NO_x and NH₃
131 over China. REAS v1.1 is believed to be the first inventory of integrating past, present and future

132 dataset in Asia based on a consistent methodology. The REAS datasets have been validated by several
133 emissions, and denote agreement with the recent growth status in Chinese emissions (Ohara et al.,
134 2007). We also collected NO_x and NH₃ emission data from EDGAR (Emissions Database for Global
135 Atmospheric Research) v4.3.1, which was developed by the Netherlands Environmental Assessment
136 Agency and European Commission Joint Research Centre (Jg et al., 2002). The EDGAR emissions are
137 calculated on the basis of a point emissions inventory conducted by the International Energy Agency.
138 EDGAR also has a long time period 1980-2010 with the highest spatial resolution globally (0.1 °×0.1 °)
139 (<http://edgar.jrc.ec.europa.eu/overview.php?v=431>).

140 **2.2. Satellite observations**

141 IASI is a passive remote-sensing instrument operating in nadir mode and measures the infrared
142 radiation emitted by the Earth's surface and the atmosphere (Clarisse et al., 2009). It covers the entire
143 globe twice a day, crossing the equator at a mean solar local time of 9:30 A.M. and P.M. and has an
144 elliptical footprint of 12 by 12 km up to 20 by 39 km depending on the satellite-viewing angle. In this
145 study we use daytime satellite observations as these are more sensitive to NH₃ and are associated with a
146 large positive thermal contrast and a significant amount of NH₃ (Van Damme et al., 2014b; Whitburn et
147 al., 2016a). The availability of measurements is mainly driven by the cloud coverage as only
148 observations with cloud coverage lower than 25% are processed to be a good compromise between the
149 number of data kept for the analysis and the bias due to the effect of clouds. As the amount of daily
150 data is not always sufficient to obtain meaningful distributions (due to cloud cover or the availability of
151 the temperature profiles from the EUMETSAT operational processing chain) (Van Damme et al.,
152 2014b), it is more appropriate to consider monthly or yearly averages for this trend analysis. We
153 consider IASI observations with a relative error below 100% or an absolute error below 5×10^{15} molec.

154 cm^{-2} for analysis over China. For the error, the filtering depends on the use of the data. Doing this, low
155 columns typical for background conditions with a large relative error but a small absolute error are also
156 taken into account. For other applications, such as comparing with ground measurements, we would
157 recommend to use a threshold of 75% or even 100% relative error. We gained the data upon request
158 from the Atmospheric Spectroscopy Group at Université Libre De Bruxelles
159 (<http://www.ulb.ac.be/cpm/atmosphere.html>). This data can be gridded on 0.1° latitude \times 0.1° longitude
160 (Dammers et al., 2016), 0.25° latitude \times 0.25° longitude (Whitburn et al., 2016a) and 0.5° latitude \times 0.5°
161 longitude (Whitburn et al., 2016b) or even coarser resolutions depending on the usage of the data. For
162 IASI NH_3 , we firstly divided China into 0.5° latitude \times 0.5° longitude grid. For each grid cell, we
163 calculated the monthly arithmetic mean by averaging the daily values with observations points within
164 the grid cell. Similarly, we calculated the annual arithmetic mean by averaging the daily values with
165 observations points within the grid cell over the whole year.

166 The NO_2 columns are obtained from the OMI instrument on NASA's EOS Aura satellite globally
167 everyday. We used the generated products by the project "Derivation of Ozone Monitoring Instrument
168 tropospheric NO_2 in near-real time" (DOMINO) to analyze the temporal trends of NO_2 columns over
169 China. In DOMINO products, only the observations with a cloud radiance fraction below 0.5 were
170 processed for analysis. The retrieval algorithm is described in detail in the previous work (Boersma et
171 al., 2007) and recent updates can be found in the DOMINO Product Specification Document
172 (http://www.temis.nl/docs/OMI_NO2_HE5_1.0.2.pdf). We used tropospheric NO_2 retrievals from the
173 DOMINO algorithm v2.0. The retrieval quality of NO_2 products is strongly dependent on different
174 aspects of air mass factors, such as radiative transfer calculations, terrain heights and surface albedo.
175 The OMI v2.0 data were mainly improved by more realistic atmospheric profile parameters, and

176 include more surface albedo and surface pressure reference points than before (Boersma et al.,
177 2011;Boersma et al., 2016). The DOMINO NO₂ datasets are available from
178 <http://www.temis.nl/airpollution/no2.html>. We should state in particular that we used directly the
179 DOMINO v2.0 products of monthly means from 2005 to 2015 over China for the trend analysis. The
180 DOMINO NO₂ columns were gridded at a resolution of 0.125 °latitude×0.125 °longitude grid globally,
181 which has been widely used for scientific applications (Ma et al., 2013;Ialongo et al., 2016;Castellanos
182 et al., 2015).

183 To illustrate measurement availability, we presented here some measurement statistics. A total number
184 of cloud-free daytime observations as characterized by the operational IASI processor by year were
185 retrieved in China during 2008-2015 for NH₃ (Fig. 1b). We retrieved more observation numbers after
186 2010 than those during 2008-2009. In 2010, the update of the improved air temperature profiles, cloud
187 properties products and cloud detection, which are important for calculating the thermal contrast,
188 increased the quality of retrieval (Van Damme et al., 2014b;Van Damme et al., 2014c). In September
189 2014, there was another update of the air temperature profiles, cloud properties products and cloud
190 detection for calculating the thermal contrast. For the updates of the IASI-NH₃ data, you can refer to
191 Van Damme et al. (2014b), Van Damme et al. (2014c) and Whitburn et al. (2016). The monthly
192 observation numbers are also presented in Fig. 1a, showing that spring (Mar, Apr and May), summer
193 (Jun, Jul and Aug), autumn (Sep, Oct and Nov) and winter (Dec, Jan and Feb) months represent 29% ,
194 26%, 23% and 21%, respectively. Compared with large variations of observation numbers for NH₃, the
195 observation numbers for NO₂ varied less by year; winter season had the least, while other seasons
196 varied little.

197 **2.3. Atmospheric transport chemistry model**

198 Atmospheric transport chemistry model is also of central importance in modeling the tropospheric NO₂
199 and NH₃. We applied a widely used atmospheric global atmospheric transport chemistry model named
200 as the Model for Ozone and Related chemical Tracers, version 4 (MOZART-4) to simulate the
201 tropospheric NO₂ and NH₃ columns during 2008-2015 in accordance with the time period of IASI NH₃
202 measurements.

203 The MOZART-4 model is driven by the meteorological data from the NASA Goddard Earth Observing
204 System Model, Version 5 (GEOS-5) at a resolution of 1.9° latitude × 2.5° longitude spatially. The
205 emission data applied for driving the simulations are based on the updated EDGAR emission
206 inventories. 12 bulk aerosol compounds, 39 photolysis, 85 gas species as well as 157 gas-phase
207 reactions were integrated in MOZART-4. The chemical mechanism on N compounds including the NO₂,
208 NH₃ and aerosols are detailedly integrated to MOZART-4, which is considered to be suitable for
209 tropospheric chemical compositions (Emmons et al., 2010; Pfister et al., 2008; Sahu et al., 2013). The
210 output data used in the current work are temporally varying six hours every day, which were upon
211 request by Louisa Emmons at National Center for Atmospheric Research (NCAR). The monthly means
212 of NO₂ and NH₃ columns were averaged by the daily data, and then used for the trend analysis over
213 China. For more details about MOZART-4, the reader should refer to previous studies (Emmons et al.,
214 2010; Brasseur et al., 1998; Beig and Singh, 2007).

215 **3. Results and discussions**

216 **3.1. NH₃ and NO₂ emissions during 1980-2010**

217 We conducted the temporal analysis of NH₃ and NO_x emissions since 1980 based on REAS and
218 EDGAR. Both significant continuous increasing trends of NH₃ and NO_x were observed from REAS

219 (for NH_3 $0.17 \text{ kg N ha}^{-1} \text{ y}^{-2}$ and for NO_x $0.16 \text{ kg N ha}^{-1} \text{ y}^{-2}$) and EDGAR (for NH_3 $0.24 \text{ kg N ha}^{-1} \text{ y}^{-2}$
220 and for NO_x $0.17 \text{ kg N ha}^{-1} \text{ y}^{-2}$) over China (Fig. 2). We found a relatively consistent increase in NO_x
221 emission from EDGAR and REAS over China, i.e. $0.17 \text{ kg N ha}^{-1} \text{ y}^{-2}$ vs $0.16 \text{ kg N ha}^{-1} \text{ y}^{-2}$, but
222 inconsistency in the magnitude of NH_3 emissions from EDGAR and REAS over China, i.e. 0.24 kg N
223 $\text{ha}^{-1} \text{ y}^{-2}$ vs $0.17 \text{ kg N ha}^{-1} \text{ y}^{-2}$. The increase rate in NH_3 emissions over China from EDGAR was much
224 higher than that from REAS, indicating the magnitude of increase trend in NH_3 over China remains a
225 debate, although their trend values of $0.24 \text{ kg N ha}^{-1} \text{ y}^{-2}$ (EDGAR) vs $0.17 \text{ kg N ha}^{-1} \text{ y}^{-2}$ (REAS) both
226 reflected a continuous increasing trend (in this regard they are consistent). It implies that, at least, the
227 NH_3 emissions are indeed increasing during 1980-2010. We also conducted a simple correlation
228 analysis of the NH_3 (Fig. 2a) and NO_x (Fig. 2b) from REAS and EDGAR, showing agreement in the
229 magnitude (slope=1.06) and temporal trend ($R^2=0.96$) for NO_x , but some inconsistency in the increase
230 rate (slope=1.33) for NH_3 .

231 The discrepancy in the magnitude of NH_3 increase rate from REAS and EDGAR ($0.24 \text{ kg N ha}^{-1} \text{ y}^{-2}$ vs
232 $0.17 \text{ kg N ha}^{-1} \text{ y}^{-2}$) in China since 1980 may be caused by the different emission factors considered for
233 estimating NH_3 emissions. The EDGAR v4.3.1 NH_3 emissions were calculated based on a variety of
234 sectors including agriculture, shipping, waste solid and wastewater, energy for buildings, process
235 emissions during production and application, power industry, oil refineries, transformation industry,
236 combustion for manufacturing, road transportation, railways, pipelines and off-road transport, while the
237 REAS v1.1 NH_3 emissions focused mainly on the agriculture source (i.e., manure management of
238 livestock and fertilizer application) (Crippa et al., 2015; Ohara et al., 2007). Moreover, the fundamental
239 methodology on estimating the REAS v1.1 NH_3 emissions did not consider the seasonal agricultural
240 variations compared with that of EDGAR v4.3.1 NH_3 emissions (Kurokawa et al., 2013), and the

241 removal efficiency (as a key element to estimate NH₃ emissions) was also reported to be much higher
242 in REAS v1.1 than in EDGAR v4.3.1 (Kurokawa et al., 2013).

243 A previous study (Liu et al., 2013) summarized published data on the national anthropogenic NH₃ and
244 NO_x emissions with multi-periods in China (Wang et al., 2009; Wang et al., 1997; Streets et al.,
245 2003; Klimont et al., 2001; Sun and Wang, 1997; Olivier et al., 1998; FRCGC, 2007), and also analyzed
246 the temporal pattern of NH₃ emissions. Their results showed that the NH₃ emissions had increased at an
247 annual average rate of 0.32 Tg N y⁻² (about 0.33 kg N ha⁻¹ y⁻²). The increase rate of NH₃ emissions
248 (0.33 kg N ha⁻¹ y⁻²) by Liu et al. (2013) was double that in REAS (0.17 kg N ha⁻¹ y⁻²), implying that the
249 NH₃ increase rate in China is still an open question, and should be further studied.

250 **3.2. Satellite NH₃ and NO₂ over China in the recent decade**

251 **3.2.1. Temporal trends**

252 We referred to the method of a previous study (Russell et al., 2012) to conduct the temporal trend
253 analysis by calculating the average values during cold months (October-March) and warm months
254 (April-September) respectively. We herein concentrated more on the temporal analysis of satellite
255 observations during warm months because of the relatively lower uncertainty in comparison with that
256 during cold months. Fig. 3 shows the temporal trend of NO₂ columns during warm and cold months
257 between 2005 and 2015 as well as monthly average values. From satellite observations, the NO₂
258 columns over China increased with a slope of 0.063×10^{15} molec. cm⁻² y⁻¹ (4.07% y⁻¹) in warm months
259 from 2005 to 2011 and then decreased with a slope of -0.072 molec. cm⁻² in warm months (-3.62% y⁻¹)
260 from 2011 to 2015 (Fig. 3). The decreasing trends were consistent with NO_x emissions since 2011 over
261 China (decreasing from 24.04×10^6 ton in 2011 to 20.78×10^6 ton in 2014, China Statistical Yearbook,
262 <http://www.stats.gov.cn/>). During the Chinese 11th Five-Year-Plan (FYP) period (2006-2010), Chinese

263 government undertook a series of strategies to increase energy efficiency and to reduce NO_x emissions,
264 but NO_x emissions were not successfully restrained, which created a big challenge for improving air
265 quality over the country (Xia et al., 2016). During the 12th FYP period (2011-2015), more stringent
266 strategies were implemented to control NO_x emissions, including the application of selective
267 catalytic/non-catalytic reduction (SCR/SNCR) systems in the power sector, staged implementation of
268 tighter vehicle emission standards and a series of standards with aggressive emission limits for power,
269 cement, and the iron and steel industries. These strategies are believed to have helped achieve national
270 targets of NO_x emission abatement (Xia et al., 2016).

271 However, the satellite-retrieved NH₃ columns increased with a slope of 0.118×10^{15} molec. cm⁻² y⁻¹
272 (2.37% y⁻¹) in warm months from 2008 to 2014 (Fig. 3), but increase largely in 2015 (this will be
273 discussed in Sect. 3.3 in comparison with MOZART-4 simulations in detail). The percent increase rate
274 for NH₃ by year (2.37% y⁻¹) from 2008 to 2014 is lower than that for NO₂ (4.07% y⁻¹) from 2005 to
275 2011, although the absolute NH₃ increase rate of 0.118×10^{15} molec. cm⁻² y⁻¹ from 2008 to 2014 was
276 higher than absolute NO₂ increase rate of 0.063×10^{15} molec. cm⁻² y⁻¹ from 2005 to 2011. An increase in
277 NH₃ columns from IASI may be due to decreased NH₃ removal leading to a larger fraction maintaining
278 in gaseous state for a long time rather than changing to the condensed phase. Specifically, NH₃ is
279 considered as an important alkaline gas that is abundant in the atmosphere, and is able to neutralize
280 acidic components including HNO₃ and H₂SO₄ through the oxidation of NO_x and SO₂, respectively (Li
281 et al., 2014; Liu et al., 2011; Liu et al., 2017c; Xu et al., 2015). The decreased NH₃ removal to some
282 degree can be attributed to continuous decreased acidic gases including the NO₂ and SO₂ over China
283 under strong control policy in 12-th FYP, which can largely decrease the fraction of the chemical
284 conversion to (NH₄)₂SO₄ and NH₄NO₃ in the atmosphere. Increasing trend in NH₃ columns may be

285 associated with continuous N fertilizer use for guaranteeing increase of crop productions (Erisman et
286 al., 2008). Although there was no strong NH₃ emission control regulation, N fertilizer efficiency should
287 be further improved over China. In 2015, the Ministry of Agriculture formally announced a “Zero
288 Increase Action Plan” for national fertilizer use by 2020, which requires the annual increase in total
289 fertilizer use will be less than 1% from 2015 to 2019, with no further increment from 2020 (Liu et al.,
290 2015).

291 If the “Zero Increase Action Plan” for N fertilizer can be effective, future NH₃ emissions should be
292 consistent with the current NH₃ emissions. In addition, due to strong emission control of NO_x, the NO_x
293 emissions were believed to decrease significantly from 2011 to 2015. We can reasonably make two
294 major conclusions. First, the atmospheric NO₂, as a key indicator of oxidized N compounds (NO₂,
295 HNO₃ and NO₃⁻), decreased since 2011, and will continue to decrease under the current policy. Second,
296 the atmospheric NH₃, as a key indicator of reduced N (NH₃ and particulate NH₄⁺), will slightly increase
297 or stay at the current level in the future with the “Zero Increase Action Plan”. Thus, due to a decreasing
298 trend of oxidized N (NO_x-N), ammonia N (NH_x-N) should still dominate Nr deposition (oxidized N
299 plus reduced N) in China, and is expected to play a more significant role in Nr deposition. Therefore,
300 monitoring the reduced N on a regional scale is encouraged to assist in enacting effective measures to
301 protect the environments and public health, with respect to air, soil and water quality.

302 **3.2.2. Spatial pattern**

303 High NH₃ columns were found in Beijing, Hebei, Henan, Shandong, Hubei and Jiangsu provinces and
304 in Eastern Sichuan province (Fig. 4a), which were consistent with their high NH₃ emissions due to
305 intensive fertilizer application and livestock (Huang et al., 2012). Guangdong, Guangxi, Hunan and
306 Jiangxi provinces also showed high NH₃ columns, due to high volatilization from paddy fields in these

307 regions, with rice being the dominant crop and contributing the most emissions. High NH₃ columns in
308 southern China are in agreement with the high percent paddy farmland area (Fig. S1a) and the high
309 NH₃ columns in northern China are in agreement with the high percent dry farmland area (Fig. S1b). In
310 addition, the NH₃ emissions from vehicles in urban areas could also contribute to the observed high
311 NH₃ columns. For example, in Beijing, the contribution of vehicles equipped with catalytic converters,
312 particularly since the introduction of three-way-catalysts, to non-agricultural NH₃ emissions has
313 recently been considered and might be the most important factor influencing NH₃ concentrations in
314 urban cities (Meng et al., 2011; Xu et al., 2017). In addition, Xinjiang province also emits remarkable
315 NH₃ emissions related to sheep manure management (Huang et al., 2012; Kang et al., 2016; Zhou et al.,
316 2015; Liu et al., 2017a). The lower NH₃ columns are located mostly in the Tibet Plateau area, where
317 there is a minimal amount of arable land and low use of synthetic nitrogenous fertilizers.

318 NO₂ columns (Fig. 4b) show significantly higher values over vast areas covering North China, East
319 China, and the Sichuan Basin. The NO₂ columns also show high values over the Pearl River Delta, the
320 southern part of Northeast China, and some areas in Northwest China. High NO₂ columns are mostly
321 distributed in populated areas (Fig. S2), where there is a mix of various anthropogenic NO_x sources,
322 such as vehicles and industrial complexes (Wang et al., 2012; Xu et al., 2015; Meng et al., 2010). It
323 should be noted that an enhanced emission intensity from transportation is confirmed since 2005, even
324 with staged implementation of tightened emission standards for on-road vehicles (Wang et al., 2012).

325 For example, NO_x emissions from transportation grew to 30% for the whole country in 2014, and the
326 values reached 44%, 55%, and 33% for Beijing, Shanghai, and Guangdong, respectively (Xia et al.,
327 2016). Therefore, transportation is believed to play an increasingly important role in regional NO₂
328 pollution, especially when emissions from stationary sources are gradually controlled through increased

329 penetration of selective catalytic/non-catalytic reduction (SCR/SNCR) systems.

330 **3.2.3. Limitations of satellite observations**

331 It is difficult to gain whole coverage over China based on the daily data for both IASI NH₃ and OMI
332 NO₂. For daily NO₂, the spatial coverage gained by OMI were influenced by cloud radiance fractions,
333 surface albedo, solar zenith angles, row anomaly and so on (Russell et al., 2011;De Smedt et al., 2015).
334 "Row anomaly" issue resulting from the OMI instrumental problem had an impact on approximately
335 half of the rows undergoing unpredictable patterns in cross-track directions relying on latitudes and
336 seasons and prevented obtaining convincing daily product with continuous coverage (Boersma et al.,
337 2011;Boersma et al., 2016). For NH₃, the satellite instruments were strongly dependent on the
338 meteorological conditions such as cloud fractions or the availability of the temperature profiles (Van
339 Damme et al., 2014b;Boersma et al., 2011), and we cannot retrieve the whole coverage based on daily
340 data over China. It will be beneficial to analyze a very local region with enough numbers of
341 observations, but not appropriate to analyze such large coverage over China.

342 Facing this big challenge, we used the monthly data for the trend analysis over China. The uncertainty
343 of DOMINO v2.0 NO₂ columns has been well documented in Boersma et al. (2011), and the relative
344 error is reported lower than 20-30% in East Asian by an improved altitude-dependent air mass factor
345 look-up table, a more realistic atmospheric profile, an increased number of reference vertical layers and
346 advanced surface albedos (Boersma et al., 2011). The reader is strongly suggested to refer to Boersma
347 et al. (2011) for more details on the uncertainty analysis.

348 The potential uncertainty of IASI NH₃ columns resulted from IASI observation instruments and
349 retrieval algorithms. In this paper, the NH₃ datasets were generated based on the recent-updated robust
350 and flexible NH₃ retrieval algorithms, which were designed to overcome some shortcomings of the

351 current algorithms (Whitburn et al., 2016a). The current algorithms were designed firstly to calculate
352 the hyperspectral range index (HRI), a measure for the NH₃ signature strength in the spectrum, and
353 then converted to IASI NH₃ columns by using the thermal contrast (TC) and lookup tables (LUT) of
354 (HRI, TC) pair corresponding to NH₃ columns. The retrieval of HRIs is strongly dependent on the
355 amount of NH₃ and the thermal state of the atmosphere (Whitburn et al., 2016a). The quality of the
356 IASI NH₃ product has been validated by atmospheric chemistry transport models, ground-based and
357 airborne measurements, and NH₃ total columns obtained with ground-based Fourier transform infrared
358 spectroscopy (FTIR). A first validation of the IASI NH₃ using the LOTOS-EUROS model was
359 conducted over Europe, indicating the respective consistency of IASI measurements and model
360 simulations (Van Damme et al., 2014c). A first evaluation of IASI NH₃ dataset using ground-based
361 measurements was made worldwide, presenting consistency with the available ground-based
362 observations and denoting promising results for evaluation by using independent airborne data (Van
363 Damme et al., 2014a). A first validation of of IASI NH₃ dataset using ground-based FTIR derived NH₃
364 total columns was evaluated, demonstrating a mean relative difference of $-32.4\pm(56.3)\%$, a correlation
365 r of 0.8 with a slope of 0.73 (Dammers et al., 2016).

366 **3.3. Atmospheric chemistry transport model NO₂ and NH₃ columns since 2008**

367 Satellite NO₂ and NH₃ columns were observed at overpass time as an instantaneous point in a day (at
368 9:30 A.M. for IASI NH₃ and at 1:45 P.M. for OMI NO₂ local time). These instantaneous satellite
369 observations may not be representative for the temporal trend analysis over China. We further retrieved
370 the monthly variations of NO₂ and NH₃ columns since 2008 from MOZART varying 6 hours every day
371 (00, 06, 12, 18 h). We compared the temporal trend analysis of NO₂ from MOZART at 12 h with that
372 gained from satellite at the overpass time (OMI 1:45 P.M. local time) as well as for NH₃.

373 Fig. 5 shows the NO₂ columns at 12:00 during warm and cold months between 2008 and 2015 from
374 MOZART. The percent increase rate for NO₂ columns at 12:00 during warm months (April-September)
375 between 2008 and 2011 was 4.02% y⁻¹ (Fig. 5), which was comparable with that (4.23% y⁻¹) derived
376 from OMI (Fig. 3). During 2011-2015, we found a slightly lower decrease rate (-2.93% y⁻¹) in NO₂
377 columns during warm months at 12:00 from MOZART (Fig. 5) than that (-3.62% y⁻¹) gained from OMI
378 at 13:45 (Fig. 3). The temporal variations of NO₂ columns at 12:00 from MOZART were generally in
379 accord with those from OMI at 13:45 P.M. local time. Fig. 5 also demonstrates the average NO₂
380 columns (averaged at 00, 06, 12 and 18 h) during warm and cold months between 2008 and 2015. We
381 found a close increase rate at 12:00 (4.02%) with that averaged at 00, 06, 12 and 18 h (4.23%) before
382 2011, as well as a similar decrease rate at 12:00 (-2.93%) and the average (-3.07%), implying that the
383 temporal trend analysis at 12:00 vs. that averaged at 00, 06, 12 and 18 h can be considered mostly
384 consistent over China from MOZART.

385 For NH₃, we found the percent increase rate at 12:00 during warm months between 2008 and 2015 was
386 1.30% y⁻¹ from MOZART (Fig. 5), which was lower than that (2.37% y⁻¹) from IASI during 2008-2014.
387 The percent increase rate by daily average (at 00, 06, 12 and 18 h) during warm months between 2008
388 and 2015 was 1.36% y⁻¹ from MOZART (Fig. 5). In 2015, we found a relatively large increase in NH₃
389 columns in China during warm months between 2014 and 2015 (50.45%) from IASI, while an increase
390 from MOZART was about 8.13% between 2014 and 2015. In MOZART-4, the alkaline gaseous NH₃
391 and the acidic gaseous NO₂ (the precursor for HNO₃) and SO₂ are very important precursors for bulk
392 NH₄NO₃ and (NH₄)₂SO₄ particles, which form the primary system of gas-particle partitioning
393 (NH₃-NH₄⁺-NO_x-NO₃⁻-SO₂-SO₄²⁻). The chemical shifts between particulate NH₄NO₃ and gaseous NH₃
394 and NO_x are correlated with the abundance of NH₃ and NO_x and meteorological factors. The decreased

395 abundance of NO_x between 2011 and 2015 may also contribute to an increase in the NH_3 abundance in
396 the gas stage resulting from decreased conversion to particulate NH_4NO_3 .

397 Large difference in the NH_3 increase rate in 2015 was found between IASI (50.45%) and MOZART
398 (8.13%). This may be still an open question on this point, here we only show this two possibilities. We
399 should clarify in particular we do not aim at validating which is right or wrong from IASI and
400 MOZART (which may be beyond the discussion in this paper), but the NH_3 columns in 2015 indeed
401 increased both from IASI and MOZART. At the current state, we can, at least, draw a conclusion that
402 the NH_3 columns over China indeed increased in 2015 both from IASI and MOZART, but a debate or
403 inconsistency exists on the increase rate of the NH_3 columns in 2015. We should state in particular
404 again that the following discussion in this paragraph was all hypothetical and should be tested in the
405 future work. For IASI NH_3 columns, the sharp increase in 2015 over China may be an artifact, which
406 may be due to an update of the input data. Similar jumps in IASI NH_3 increase in 2015 can also be
407 visible in the USA and European (Fig. 6), indicating that it may be necessary for a recalculation of the
408 earlier input datasets used for calculating the IASI NH_3 columns since September, 2014.

409 **3.4. Implications for estimating long-term Nr deposition datasets and recommendations for** 410 **future work**

411 We found both the NO_x and NH_3 over China increased continuously from 1980 to 2010 based on
412 emissions data from REAS and EDGAR. In recent years, based on satellite observations, we found an
413 increase of $2.37\% \text{ y}^{-1}$ in NH_3 columns during 2008-2014. We also found high-level NO_2 columns over
414 China from 2005-2011 ($4.07\% \text{ y}^{-1}$) but a decrease from 2011 to 2015 ($-3.62\% \text{ y}^{-1}$). Despite the decline,
415 the NO_2 columns during 2011-2015 were still in high level with an average of $1.87 \times 10^{15} \text{ molec. cm}^{-2}$
416 y^{-1} compared with that ($1.65 \times 10^{15} \text{ molec. cm}^{-2} \text{ y}^{-1}$) during 2005-2010. Notably, these emissions

417 certainly lead to the deposition of atmospheric Nr in form of dry and wet processes into aquatic
418 ecosystems and terrestrial, with implications affecting ecosystem and human health, biological
419 diversity and greenhouse gas balances (Lu et al., 2016). Hence, it is very crucial to estimate Nr
420 deposition with high spatiotemporal resolutions in order to drive ecological models such as the
421 Denitrification-Decomposition (DNDC) model and Integrated Biosphere Simulator (IBIS), to assess its
422 impact on soil, forest, water and greenhouse balance. Here, we call for a long-term dataset of Nr
423 depositions both regionally and globally to investigate how the N emissions affect the environment.
424 Challenge still exists in estimating both the dry (NO_2 , HNO_3 particulate NO_3^- , NH_3 and particulate NH_4^+)
425 and wet (NH_4^+ and NO_3^- in precipitation) depositions for a long-term dataset such as since 1980 or
426 earlier possibly due to the complex scheme of N transformations and transportation or limited available
427 data both from emissions, satellites and a limited number of ground measurements.

428 Satellite observations provide a new perspective of estimating Nr depositions regionally, and have been
429 used to improve the estimation performance. For example, to improve the modeling performance in dry
430 gaseous NO_2 depositions from GEOS-Chem (Goddard Earth Observing System chemical transport
431 model), Nowlan et al. (2014) applied the OMI NO_2 columns to calibrate the simulated ground NO_2
432 concentrations, and then estimated the deposition between 2005 and 2007. Our previous work focusing
433 on the dry particulate NO_3^- deposition over China was also based on the OMI NO_2 columns, MOZART
434 simulations and monitored-based sources (Liu et al., 2017b). Geddes et al. (2017) used the satellite
435 NO_2 columns from GOME, GOME-2 and SCIAMACHY instruments to calibrate the NO_x emissions in
436 GEOS-Chem to estimate the NO_x depositions since 1996. The simulations combining the satellite
437 measurements and CTM models to derive Nr depositions (Geddes and Martin, 2017; Nowlan et al.,
438 2014) in recent years will provide relatively accurate datasets (certainly need to be validated and

439 modified by ground measurements).

440 Despite progress in satellite techniques in recent decades (for NO_2 since 1997 by GOME and for NH_3
441 since 2008 by IASI), we can hardly tracked studies concerning Nr depositions before 1997 based on
442 satellite observations. Thus, with the help of emissions data such as REAS and EDGAR, we can derive
443 long-term Nr depositions, especially before 1997. Long-term emissions data such as REAS and
444 EDGAR will provide valuable dataset to expand the modeling Nr depositions in recent years. In order
445 to derive the Nr depositions from the emission data, CTMs are frequently used through modeling the
446 wet (simplified as the product of scavenging efficiency and precipitation amount) and dry process
447 (simplified as the inferential method by multiplying the deposition velocity and gaseous or particulate
448 concentrations). However, we still lack a comprehensive dataset of gridded long-term Nr depositions
449 including both the dry (NO_2 , HNO_3 particulate NO_3^- , NH_3 and particulate NH_4^+) and wet (NH_4^+ and
450 NO_3^- in precipitation) processes over China, which will be addressed in future work.

451 Another gap is that, all the above mentioned studies focused on the NO_x depositions and did not derive
452 the NH_y (NH_3 and NH_4^+) depositions over China. Our recent work (Liu et al., 2017a) using IASI NH_3
453 columns combining the vertical profiles from MOZART benefits our understanding of the ground NH_3
454 concentrations over China, and the satellite-derived ground NH_3 concentrations were generally in
455 accord with the national measurements from NNDMN. To date, there are still no reports of using the
456 satellite NH_3 columns to derive the temporal and regional NH_y depositions over China, which
457 dominated the total Nr depositions (NO_x plus NH_y) (Liu et al., 2016b; Liu et al., 2013). The gaps of
458 modeling NH_y depositions by applying the satellite observations combining the CTMs simulations
459 require more efforts and further research.

460 **4. Conclusion**

461 Atmospheric ammonia (NH₃) and nitrogen dioxide (NO₂) play an important role in determining air
462 quality, environmental degradation and climate change. The emission data, satellite observations and
463 atmospheric transport modeling have great potential for understanding the temporal variations of
464 atmospheric NH₃ and NO₂ on a regional scale, with high spatial and temporal resolutions. This study
465 analyzed the characteristics of atmospheric NH₃ and NO₂ over China since 1980 based on the multiple
466 datasets. The major findings were as follows:

467 1. Based on emission data, both significant continuous increasing trend of NH₃ and NO_x were observed
468 from REAS (for NH₃ 0.17 kg N ha⁻¹ y⁻² and for NO_x 0.16 kg N ha⁻¹ y⁻²) and EDGAR (for NH₃ 0.24 kg
469 N ha⁻¹ y⁻² and for NO_x 0.17 kg N ha⁻¹ y⁻²) over China during 1980-2010.

470 2. Based on the satellite observations, we found high-level NH₃ columns with the percent increase rate
471 of 2.37% y⁻¹ from 2008 to 2014. For NO₂, we found continuous high-level NO₂ columns over China
472 from 2005-2011 but a decrease from 2011 to 2015 (still in high level). The decrease of NO₂ columns
473 may result from more stringent strategies taken to control NO_x emissions during the 12th
474 Five-Year-Plan, including successful application of SCR/SNCR systems in the power sector, tighter
475 emission standards on vehicles and a series of standards with aggressive emission limits. Increasing
476 trend of NH₃ columns may be due to continuous N fertilizer use for guaranteeing continuous increase
477 of the crop productions. An increase in NH₃ columns may be due to decreased NH₃ removal leading to
478 a larger fraction maintaining in gaseous state for a long time rather than changing to the condensed
479 phase, which may be related with continuous decreased acidic gases including the NO₂ and SO₂ over
480 China under strong control policy in 12-th FYP.

481 3. Based on MOZART simulations, the temporal variations of NO₂ columns at 12:00 from MOZART
482 were generally in accord with those from OMI at 13:45 P.M. local time. We also found a close increase
483 rate at 12:00 (4.02%) with that averaged at 00, 06, 12 and 18 h (4.23%) before 2011, as well as a
484 similar decrease rate at 12:00 (-2.93%) and the average (-3.07%). For NH₃, we found a lower percent
485 increase rate from MOZART (1.30% y⁻¹) than IASI (2.37% y⁻¹) between 2008 and 2014. Large
486 difference in the NH₃ increase rate in 2015 was found between IASI (50.45%) and MOZART (8.13%).
487 4. The multiple datasets used in the current work have implications for estimating long-term Nr
488 deposition datasets. The simulations combining the satellite measurements and CTM models to derive
489 Nr depositions will provide relatively accurate datasets, and the REAS and EDGAR emissions have
490 potential to expand the modeling Nr depositions to long-term datasets. In particular, modeling NH_y
491 depositions by applying the satellite observations combining the CTMs simulations require more
492 efforts and further research.

493 **Acknowledgements**

494 We acknowledge the free use of tropospheric NO₂ column data from the OMI sensor from
495 www.temis.nl. The NH₃ data have been obtained by the Atmospheric Spectroscopy Group at Université
496 Libre de Bruxelles (ULB) (<http://www.ulb.ac.be/cpm/atmosphere.html>). S. Whitburn and M. Van
497 Damme are acknowledged for making the data available and for their help in how to use them. We also
498 thank Louisa Emmons from National Center for Atmospheric Research (NCAR) for providing the
499 MOZART output data for the trend analysis. This study is supported by the National Natural Science
500 Foundation of China (No. 41471343, 40425007 and 41101315).

501 **Reference**

502 Basto, S., Thompson, K., Phoenix, G., Sloan, V., Leake, J., and Rees, M.: Long-term nitrogen

503 deposition depletes grassland seed banks, *Nature Communication*, 6, 1-6, 10.1038/ncomms7185, 2015.

504 Beer, R., Shephard, M. W., Kulawik, S. S., Clough, S. A., Eldering, A., Bowman, K. W., Sander, S. P.,
505 Fisher, B. M., Payne, V. H., Luo, M., Osterman, G. B., and Worden, J. R.: First satellite observations of
506 lower tropospheric ammonia and methanol, *Geophysical Research Letters*, 35, n/a-n/a,
507 10.1029/2008GL033642, 2008.

508 Beig, G., and Singh, V.: Trends in tropical tropospheric column ozone from satellite data and MOZART
509 model, *Geophysical Research Letters*, 34, 2007.

510 Boersma, K., Eskes, H., Veefkind, J. P., Brinksma, E., Van Der A, R., Sneep, M., Van Den Oord, G.,
511 Levelt, P., Stammes, P., and Gleason, J.: Near-real time retrieval of tropospheric NO₂ from OMI,
512 *Atmospheric Chemistry and Physics*, 7, 2103-2118, 2007.

513 Boersma, K. F., Eskes, H. J., Dirksen, R. J., van der A, R. J., Veefkind, J. P., Stammes, P., Huijnen, V.,
514 Kleipool, Q. L., Sneep, M., Claas, J., Leitão, J., Richter, A., Zhou, Y., and Brunner, D.: An improved
515 tropospheric NO₂ column retrieval algorithm for the Ozone Monitoring Instrument, *Atmospheric*
516 *Measurement Techniques*, 4, 1905-1928, 10.5194/amt-4-1905-2011, 2011.

517 Boersma, K. F., Vinken, G. C. M., and Eskes, H. J.: Representativeness errors in comparing chemistry
518 transport and chemistry climate models with satellite UV-Vis tropospheric column retrievals, *Geosci.*
519 *Model Dev.*, 9, 875-898, 10.5194/gmd-9-875-2016, 2016.

520 Brasseur, G., Hauglustaine, D., Walters, S., Rasch, P., Müller, J. F., Granier, C., and Tie, X.: MOZART,
521 a global chemical transport model for ozone and related chemical tracers: 1. Model description, *Journal*
522 *of Geophysical Research: Atmospheres* (1984–2012), 103, 28265-28289, 1998.

523 Canfield, D. E., Glazer, A. N., and Falkowski, P. G.: The Evolution and Future of Earth's Nitrogen
524 Cycle, *Science*, 330, 192-196, 10.1126/science.1186120, 2010.

525 Castellanos, P., Boersma, K. F., Torres, O., and De Haan, J. F.: OMI tropospheric NO₂ air mass factors
526 over South America: effects of biomass burning aerosols, *Atmospheric Measurement Techniques*, 8,
527 2683-2733, 2015.

528 Clarisse, L., Clerbaux, C., Dentener, F., Hurtmans, D., and Coheur, P.-F.: Global ammonia distribution
529 derived from infrared satellite observations, *Nature Geoscience*, 2, 479-483, 2009.

530 Cofala, J., Amann, M., Klimont, Z., Kupiainen, K., and Höglund-Isaksson, L.: Scenarios of global
531 anthropogenic emissions of air pollutants and methane until 2030, *Atmospheric Environment*, 41,
532 8486-8499, <http://dx.doi.org/10.1016/j.atmosenv.2007.07.010>, 2007.

533 Coheur, P.-F., Clarisse, L., Turquety, S., Hurtmans, D., and Clerbaux, C.: IASI measurements of
534 reactive trace species in biomass burning plumes, *Atmospheric Chemistry and Physics*, 9, 5655-5667,
535 2009.

536 Crippa, M., Janssensmaenhout, G., Dentener, F., Guizzardi, D., Sindelarova, K., Muntean, M., Van
537 Dingenen, R., and Granier, C.: Forty years of improvements in European air quality: the role of EU
538 policy-industry interplay, *Atmospheric Chemistry & Physics*, 15, 322-337, 2015.

539 Damers, E., Palm, M., Van Damme, M., Vigouroux, C., Smale, D., Conway, S., Toon, G. C., Jones,
540 N., Nussbaumer, E., Warneke, T., Petri, C., Clarisse, L., Clerbaux, C., Hermans, C., Lutsch, E., Strong,
541 K., Hannigan, J. W., Nakajima, H., Morino, I., Herrera, B., Stremme, W., Grutter, M., Schaap, M.,
542 Wichink Kruit, R. J., Notholt, J., Coheur, P. F., and Erisman, J. W.: An evaluation of IASI-NH₃ with
543 ground-based Fourier transform infrared spectroscopy measurements, *Atmos. Chem. Phys.*, 16,
544 10351-10368, [10.5194/acp-16-10351-2016](https://doi.org/10.5194/acp-16-10351-2016), 2016.

545 De Smedt, I., Stavrou, T., Hendrick, F., Danckaert, T., Vlemmix, T., Pinardi, G., Theys, N., Lerot, C.,
546 Gielen, C., and Vigouroux, C.: Diurnal, seasonal and long-term variations of global formaldehyde

547 columns inferred from combined OMI and GOME-2 observations, *Atmospheric Chemistry & Physics*,
548 15, 12241-12300, 2015.

549 Emmons, L., Walters, S., Hess, P., Lamarque, J.-F., Pfister, G., Fillmore, D., Granier, C., Guenther, A.,
550 Kinnison, D., and Laepple, T.: Description and evaluation of the Model for Ozone and Related
551 chemical Tracers, version 4 (MOZART-4), *Geoscientific Model Development*, 3, 43-67, 2010.

552 Erisman, J. W., Sutton, M. A., Galloway, J., Klimont, Z., and Winiwarter, W.: How a century of
553 ammonia synthesis changed the world, *Nature Geoscience*, 1, 636-639, 2008.

554 Foy, B. D., Lu, Z., and Streets, D. G.: Satellite NO₂ retrievals suggest China has exceeded its
555 NO_x reduction goals from the twelfth Five-Year Plan, *Scientific Reports*, 6, 35912, 2016.

556 Regional Emission Inventory in Asia: <http://www.jamstec.go.jp/frsgc/research/d4/emission.htm>, 2007.

557 Fu, B., Li, S., Yu, X., Yang, P., Yu, G., Feng, R., and Zhuang, X.: Chinese ecosystem research network:
558 Progress and perspectives, *Ecological Complexity*, 7, 225-233,
559 <http://dx.doi.org/10.1016/j.ecocom.2010.02.007>, 2010.

560 Galloway, J. N., Dentener, F. J., Capone, D. G., Boyer, E. W., Howarth, R. W., Seitzinger, S. P., Asner,
561 G. P., Cleveland, C. C., Green, P. A., Holland, E. A., Karl, D. M., Michaels, A. F., Porter, J. H.,
562 Townsend, A. R., and Vösmarty, C. J.: Nitrogen Cycles: Past, Present, and Future, *Biogeochemistry*,
563 70, 153-226, 10.1007/s10533-004-0370-0, 2004.

564 Galloway, J. N., Townsend, A. R., Erisman, J. W., Bekunda, M., Cai, Z., Freney, J. R., Martinelli, L. A.,
565 Seitzinger, S. P., and Sutton, M. A.: Transformation of the Nitrogen Cycle: Recent Trends, Questions,
566 and Potential Solutions, *Science*, 320, 889-892, 10.1126/science.1136674, 2008.

567 Geddes, J. A., and Martin, R. V.: Global deposition of total reactive nitrogen oxides from 1996 to 2014
568 constrained with satellite observations of NO₂ columns, *Atmos. Chem. Phys. Discuss.*, 2017, 1-44,

569 10.5194/acp-2016-1100, 2017.

570 Huang, X., Song, Y., Li, M., Li, J., Huo, Q., Cai, X., Zhu, T., Hu, M., and Zhang, H.: A high resolution
571 ammonia emission inventory in China, *Global Biogeochemical Cycles*, 26, 1-14, 2012.

572 Ialongo, I., Herman, J., Krotkov, N., Lamsal, L., Boersma, K. F., Hovila, J., and Tamminen, J.:
573 Comparison of OMI NO₂ observations and their seasonal and weekly cycles with ground-based
574 measurements in Helsinki, 1-13, 2016.

575 Jg, O., Jjm, B., Jahw, P., Bakker, J., Ajh, V., and Jpj, B.: Applications of EDGAR Emission Database
576 for Global Atmospheric Research, Rijksinstituut Voor Volksgezondheid En Milieu Rivm, 2002.

577 Kang, Y., Liu, M., Song, Y., Huang, X., Yao, H., Cai, X., Zhang, H., Kang, L., Liu, X., Yan, X., He, H.,
578 Zhang, Q., Shao, M., and Zhu, T.: High-resolution ammonia emissions inventories in China from 1980
579 to 2012, *Atmos. Chem. Phys.*, 16, 2043-2058, 10.5194/acp-16-2043-2016, 2016.

580 Klimont, Z., Cofala, J., Schöpp, W., Amann, M., Streets, D. G., Ichikawa, Y., and Fujita, S.: Projections
581 of SO₂, NO_x, NH₃ and VOC Emissions in East Asia Up to 2030, *Water, Air, & Soil Pollution*, 130,
582 193-198, 2001.

583 Kurokawa, J., Ohara, T., Morikawa, T., and Hanayama, S.: Emissions of air pollutants and greenhouse
584 gases over Asian regions during 2000–2008: Regional Emission inventory in ASia (REAS) version 2,
585 *Atmospheric Chemistry & Physics*, 13, 10049-10123, 2013.

586 Lamsal, L. N., Duncan, B. N., Yoshida, Y., Krotkov, N. A., Pickering, K. E., Streets, D. G., and Lu, Z.:
587 U.S. NO₂ trends (2005–2013): EPA Air Quality System (AQS) data versus improved observations from
588 the Ozone Monitoring Instrument (OMI), *Atmospheric Environment*, 110, 130-143,
589 <http://dx.doi.org/10.1016/j.atmosenv.2015.03.055>, 2015.

590 Lan, Z., Jenerette, G. D., Zhan, S., Li, W., Zheng, S., and Bai, Y.: Testing the scaling effects and

591 mechanisms of N-induced biodiversity loss: evidence from a decade-long grassland experiment,
592 *Journal of Ecology*, 103, 750-760, 10.1111/1365-2745.12395, 2015.

593 Levelt, P., Stammes, P., Gleason, J., and Bucsela, E.: Near-real time retrieval of tropospheric NO₂ from
594 OMI, *Atmospheric Chemistry and Physics*, 7, 2103-2118, 2007.

595 Li, Y., Schwandner, F. M., Sewell, H. J., Zivkovich, A., Tigges, M., Raja, S., Holcomb, S., Molenaar, J.
596 V., Sherman, L., and Archuleta, C.: Observations of ammonia, nitric acid, and fine particles in a rural
597 gas production region, *Atmospheric Environment*, 83, 80-89, 2014.

598 Li, Y., Schichtel, B. A., Walker, J. T., Schwede, D. B., Chen, X., Lehmann, C. M., Puchalski, M. A.,
599 Gay, D. A., and Collett, J. L.: Increasing importance of deposition of reduced nitrogen in the United
600 States, *Proceedings of the National Academy of Sciences*, 113, 5874-5879, 2016a.

601 Li, Y., Thompson, T. M., Van Damme, M., Chen, X., Benedict, K. B., Shao, Y., Day, D., Boris, A.,
602 Sullivan, A. P., Ham, J., Whitburn, S., Clarisse, L., Coheur, P. F., and Collett Jr, J. L.: Temporal and
603 Spatial Variability of Ammonia in Urban and Agricultural Regions of Northern Colorado, United States,
604 *Atmos. Chem. Phys. Discuss.*, 2016, 1-50, 10.5194/acp-2016-1008, 2016b.

605 Liu, F., Zhang, Q., Ronald, J. v. d. A., Zheng, B., Tong, D., Yan, L., Zheng, Y., and He, K.: Recent
606 reduction in NO_x emissions over China: synthesis of satellite observations and emission inventories,
607 *Environmental Research Letters*, 11, 114002, 2016a.

608 Liu, L., Zhang, X., Wang, S., Lu, X., and Ouyang, X.: A Review of Spatial Variation of Inorganic
609 Nitrogen (N) Wet Deposition in China, *PloS one*, 11, e0146051, 2016b.

610 Liu, L., Zhang, X., Xu, W., Liu, X., Lu, X., Wang, S., Zhang, W., and Zhao, L.: Ground Ammonia
611 Concentrations over China Derived from Satellite and Atmospheric Transport Modeling, *Remote
612 Sensing*, 9, 467, 2017a.

613 Liu, L., Zhang, X., Zhang, Y., Xu, W., Liu, X., Zhang, X., Feng, J., Chen, X., Zhang, Y., Lu, X., Wang,
614 S., Zhang, W., and Zhao, L.: Dry Particulate Nitrate Deposition in China, *Environmental Science &*
615 *Technology*, 10.1021/acs.est.7b00898, 2017b.

616 Liu, X., Duan, L., Mo, J., Du, E., Shen, J., Lu, X., Zhang, Y., Zhou, X., He, C., and Zhang, F.: Nitrogen
617 deposition and its ecological impact in China: An overview, *Environmental Pollution*, 159, 2251-2264,
618 <http://dx.doi.org/10.1016/j.envpol.2010.08.002>, 2011.

619 Liu, X., Zhang, Y., Han, W., Tang, A., Shen, J., Cui, Z., Vitousek, P., Erisman, J. W., Goulding, K., and
620 Christie, P.: Enhanced nitrogen deposition over China, *Nature*, 494, 459-462, 2013.

621 Liu, X., Vitousek, P., Chang, Y., Zhang, W., Matson, P., and Zhang, F.: Evidence for a Historic Change
622 Occurring in China, *Environmental Science & Technology*, 50, 505-506, 2015.

623 Liu, X., Xu, W., Duan, L., Du, E., Pan, Y., Lu, X., Zhang, L., Wu, Z., Wang, X., and Zhang, Y.: Erratum
624 to: Atmospheric Nitrogen Emission, Deposition, and Air Quality Impacts in China: an Overview,
625 *Current Pollution Reports*, 1-1, 2017c.

626 Lu, X., Jiang, H., Liu, J., Zhang, X., Jin, J., Zhu, Q., Zhang, Z., and Peng, C.: Simulated effects of
627 nitrogen saturation on the global carbon budget using the IBIS model, *Scientific Reports*, 6, 39173,
628 10.1038/srep39173, 2016.

629 Ma, J. Z., Beirle, S., Jin, J. L., Shaiganfar, R., Yan, P., and Wagner, T.: Tropospheric NO₂ vertical
630 column densities over Beijing: results of the first three years of ground-based MAX-DOAS
631 measurements (2008–2011) and satellite validation, *Atmospheric Chemistry & Physics*, 13, 1547-1567,
632 2013.

633 Meng, Z.-Y., Xu, X.-B., Wang, T., Zhang, X.-Y., Yu, X.-L., Wang, S.-F., Lin, W.-L., Chen, Y.-Z., Jiang,
634 Y.-A., and An, X.-Q.: Ambient sulfur dioxide, nitrogen dioxide, and ammonia at ten background and

635 rural sites in China during 2007–2008, *Atmospheric Environment*, 44, 2625-2631,
636 <http://dx.doi.org/10.1016/j.atmosenv.2010.04.008>, 2010.

637 Meng, Z., Lin, W., Jiang, X., Yan, P., Wang, Y., Zhang, Y., Jia, X., and Yu, X.: Characteristics of
638 atmospheric ammonia over Beijing, China, *Atmospheric Chemistry and Physics*, 11, 6139-6151, 2011.

639 Nowlan, C., Martin, R., Philip, S., Lamsal, L., Krotkov, N., Marais, E., Wang, S., and Zhang, Q.:
640 Global dry deposition of nitrogen dioxide and sulfur dioxide inferred from space - based measurements,
641 *Global Biogeochemical Cycles*, 28, 1025-1043, 2014.

642 Ohara, T., Akimoto, H., Kurokawa, J., Horii, N., Yamaji, K., Yan, X., and Hayasaka, T.: An Asian
643 emission inventory of anthropogenic emission sources for the period 1980–2020, *Atmos. Chem.*
644 *Phys.*, 7, 4419-4444, 10.5194/acp-7-4419-2007, 2007.

645 Olivier, J. G. J., Bouwman, A. F., Hoek, K. W. V. D., and Berdowski, J. J. M.: Global air emission
646 inventories for anthropogenic sources of NO_x, NH₃ and N₂O in 1990, *Environmental Pollution*,
647 102, 135-148, 1998.

648 Pan, Y., Wang, Y., Tang, G., and Wu, D.: Wet and dry deposition of atmospheric nitrogen at ten sites in
649 Northern China, *Atmospheric Chemistry and Physics*, 12, 6515-6535, 2012.

650 Pfister, G., Emmons, L., Hess, P., Lamarque, J. F., Orlando, J., Walters, S., Guenther, A., Palmer, P., and
651 Lawrence, P.: Contribution of isoprene to chemical budgets: A model tracer study with the NCAR CTM
652 MOZART - 4, *Journal of Geophysical Research: Atmospheres* (1984–2012), 113, 2008.

653 Russell, A., Valin, L., and Cohen, R.: Trends in OMI NO₂ observations over the United States: effects
654 of emission control technology and the economic recession, *Atmospheric Chemistry and Physics*, 12,
655 12197-12209, 2012.

656 Russell, A. R., Perring, A. E., Valin, L. C., and Bucsela, E. J.: A high spatial resolution retrieval of NO

657 2 column densities from OMI: method and evaluation, *Atmospheric Chemistry & Physics*, 11,
658 12411-12440, 2011.

659 Sahu, L., Sheel, V., Kajino, M., Gunthe, S. S., Thouret, V., Nedelec, P., and Smit, H. G.: Characteristics
660 of tropospheric ozone variability over an urban site in Southeast Asia: A study based on MOZAIC and
661 MOZART vertical profiles, *Journal of Geophysical Research: Atmospheres*, 118, 8729-8747, 2013.

662 Shi, Y., Cui, S., Ju, X., Cai, Z., and Zhu, Y.-G.: Impacts of reactive nitrogen on climate change in China,
663 *Scientific Reports*, 5, 8118, 10.1038/srep08118
664 <http://www.nature.com/articles/srep08118#supplementary-information>, 2015.

665 Streets, D. G., Bond, T. C., Carmichael, G. R., Fernandes, S. D., He, D., Klimont, Z., Nelson, S. M.,
666 Tsai, N. Y., and Wang, M. Q.: An inventory of gaseous and primary aerosol emissions in Asia in the
667 year 2000, *Journal of Geophysical Research Atmospheres*, 108, GTE 30-31, 2003.

668 Sun, Q., and Wang, M.: Ammonia Emission and Concentration in the Atmosphere over China, *Scientia*
669 *Atmospherica Sinica*, 1997.

670 Van Damme, M., Clarisse, L., Dammers, E., Liu, X., Nowak, J., Clerbaux, C., Flechard, C.,
671 Galy-Lacaux, C., Xu, W., and Neuman, J.: Towards validation of ammonia (NH₃) measurements from
672 the IASI satellite, *Atmospheric Measurement Techniques*, 7, 12125-12172, 2014a.

673 Van Damme, M., Clarisse, L., Heald, C., Hurtmans, D., Ngadi, Y., Clerbaux, C., Dolman, A., Erisman,
674 J. W., and Coheur, P.-F.: Global distributions, time series and error characterization of atmospheric
675 ammonia (NH₃) from IASI satellite observations, *Atmospheric Chemistry and Physics*, 14, 2905-2922,
676 2014b.

677 Van Damme, M., Wichink Kruit, R., Schaap, M., Clarisse, L., Clerbaux, C., Coheur, P. F., Dammers, E.,
678 Dolman, A., and Erisman, J.: Evaluating 4 years of atmospheric ammonia (NH₃) over Europe using

679 IASI satellite observations and LOTOS - EUROS model results, *Journal of Geophysical Research:*
680 *Atmospheres*, 119, 9549-9566, 2014c.

681 Walker, J. C., Dudhia, A., and Carboni, E.: An effective method for the detection of trace species
682 demonstrated using the MetOp Infrared Atmospheric Sounding Interferometer, *Atmos. Meas. Tech.*, 4,
683 1567-1580, 10.5194/amt-4-1567-2011, 2011.

684 Wang, S., Zhang, Q., Streets, D., He, K., Martin, R., Lamsal, L., Chen, D., Lei, Y., and Lu, Z.: Growth
685 in NO_x emissions from power plants in China: bottom-up estimates and satellite observations,
686 *Atmospheric Chemistry and Physics*, 12, 4429-4447, 2012.

687 Wang, S. W., Liao, J. H., Yu-Ting, H. U., and Yan, X. Y.: A Preliminary Inventory of NH₃-N Emission
688 and Its Temporal and Spatial Distribution of China, *Journal of Agro-Environment Science*, 2009.

689 Wang, W. X., Lu, X. F., Pang, Y. B., Tang, D. G., and Zhang, W. H.: Geographical distribution of NH₃
690 emission intensities in China, *Actaentiae Circumstantiae*, 1997.

691 Warner, J. X., Dickerson, R. R., Wei, Z., Strow, L. L., Wang, Y., and Liang, Q.: Increased atmospheric
692 ammonia over the world's major agricultural areas detected from space, *Geophysical Research Letters*,
693 n/a-n/a, 10.1002/2016GL072305, 2017.

694 Whitburn, S., Van Damme, M., Clarisse, L., Bauduin, S., Heald, C. L., Hadji-Lazaro, J., Hurtmans, D.,
695 Zondlo, M. A., Clerbaux, C., and Coheur, P. F.: A flexible and robust neural network IASI-NH₃
696 retrieval algorithm, *Journal of Geophysical Research: Atmospheres*, 121, 6581-6599,
697 10.1002/2016JD024828, 2016a.

698 Whitburn, S., Van Damme, M., Clarisse, L., Turquety, S., Clerbaux, C., and Coheur, P. F.: Doubling of
699 annual ammonia emissions from the peat fires in Indonesia during the 2015 El Niño, *Geophysical*
700 *Research Letters*, 43, 11,007-011,014, 10.1002/2016GL070620, 2016b.

701 Wichink Kruit, R. J., Schaap, M., Sauter, F. J., van Zanten, M. C., and van Pul, W. A. J.: Modeling the
702 distribution of ammonia across Europe including bi-directional surface–atmosphere exchange,
703 *Biogeosciences*, 9, 5261-5277, [10.5194/bg-9-5261-2012](https://doi.org/10.5194/bg-9-5261-2012), 2012.

704 Xia, Y., Zhao, Y., and Nielsen, C. P.: Benefits of China's efforts in gaseous pollutant control indicated
705 by the bottom-up emissions and satellite observations 2000–2014, *Atmospheric Environment*, 136,
706 43-53, <http://dx.doi.org/10.1016/j.atmosenv.2016.04.013>, 2016.

707 Xie, Y., Zhao, B., Zhang, L., and Luo, R.: Spatiotemporal variations of PM_{2.5} and PM₁₀
708 concentrations between 31 Chinese cities and their relationships with SO₂, NO₂, CO and O₃,
709 *Particuology*, 20, 141-149, <http://dx.doi.org/10.1016/j.partic.2015.01.003>, 2015.

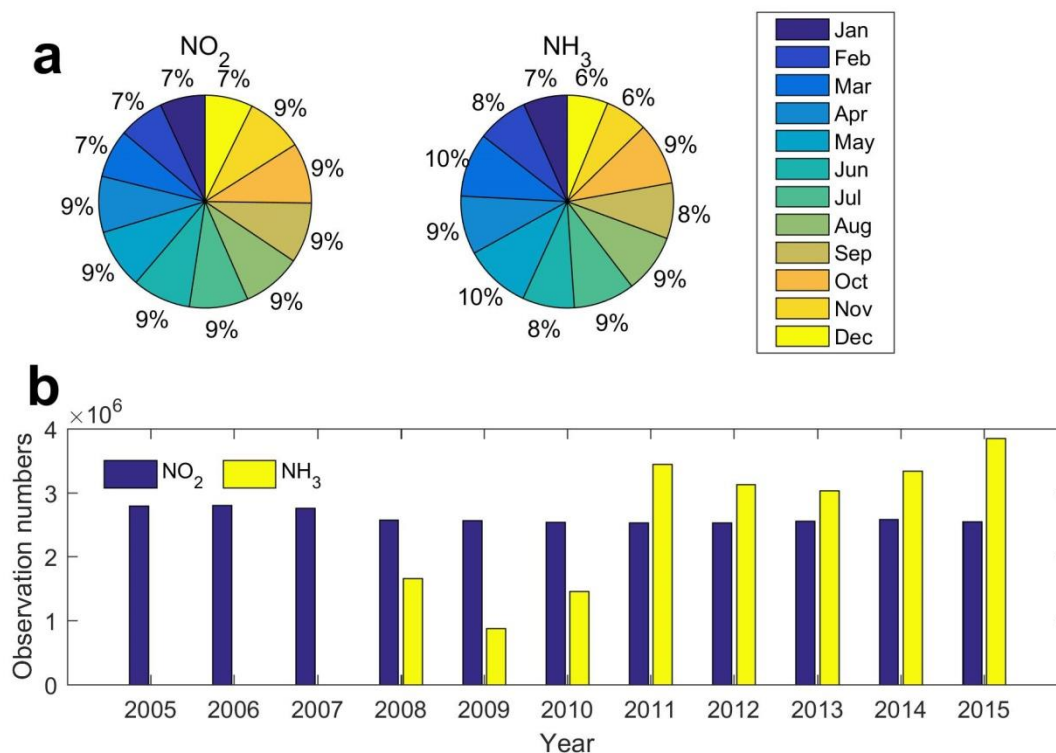
710 Xu, W., Luo, X. S., Pan, Y. P., Zhang, L., Tang, A. H., Shen, J. L., Zhang, Y., Li, K. H., Wu, Q. H., Yang,
711 D. W., Zhang, Y. Y., Xue, J., Li, W. Q., Li, Q. Q., Tang, L., Lv, S. H., Liang, T., Tong, Y. A., Liu, P.,
712 Zhang, Q., Xiong, Z. Q., Shi, X. J., Wu, L. H., Shi, W. Q., Tian, K., Zhong, X. H., Shi, K., Tang, Q. Y.,
713 Zhang, L. J., Huang, J. L., He, C. E., Kuang, F. H., Zhu, B., Liu, H., Jin, X., Xin, Y. J., Shi, X. K., Du,
714 E. Z., Dore, A. J., Tang, S., Collett Jr, J. L., Goulding, K., Sun, Y. X., Ren, J., Zhang, F. S., and Liu, X.
715 J.: Quantifying atmospheric nitrogen deposition through a nationwide monitoring network across China,
716 *Atmospheric Chemistry and Physics*, 15, 12345-12360, 2015.

717 Xu, W., Song, W., Zhang, Y., Liu, X., Zhang, L., Zhao, Y., Liu, D., Tang, A., Yang, D., and Wang, D.:
718 Air quality improvement in a megacity: implications from 2015 Beijing Parade Blue pollution control
719 actions, *Atmospheric Chemistry and Physics*, 17, 31-46, 2017.

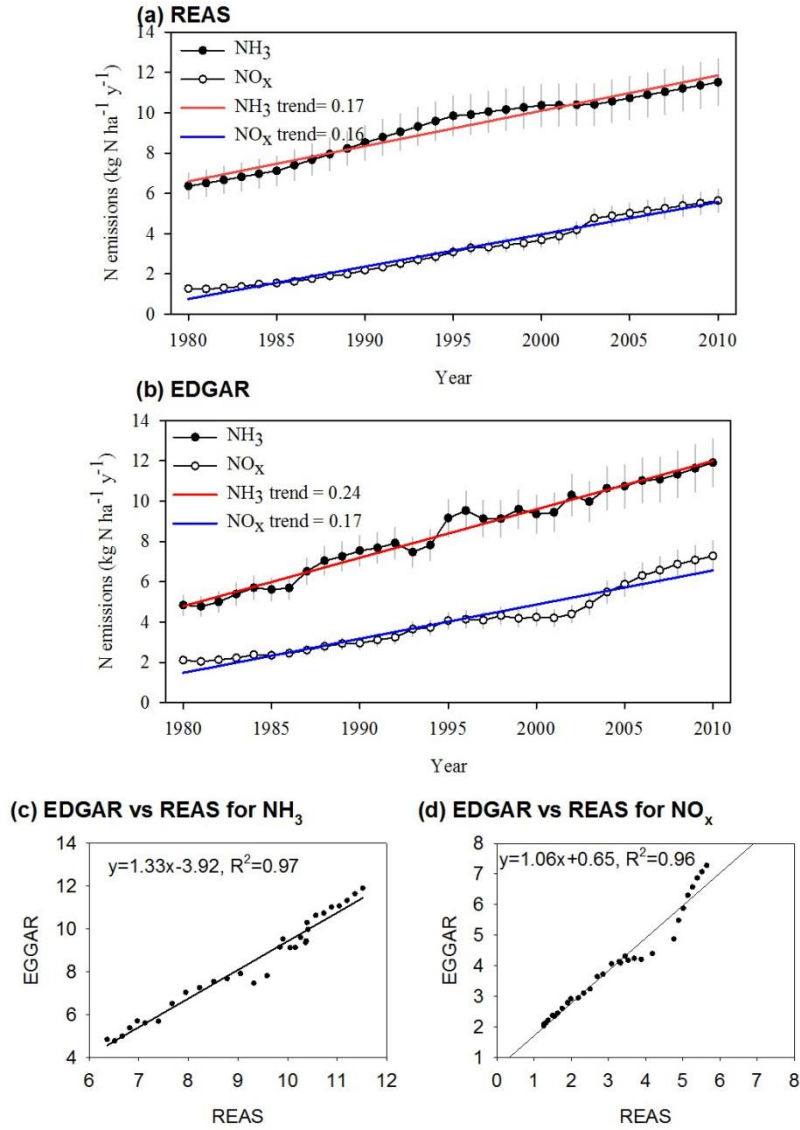
720 Zhao, C., and Wang, Y.: Assimilated inversion of NO_x emissions over east Asia using OMI NO₂
721 column measurements, *Geophysical Research Letters*, 36, 1-5, 2009.

722 Zhou, Y., Shuiyuan, C., Lang, J., Chen, D., Zhao, B., Liu, C., Xu, R., and Li, T.: A comprehensive

723 ammonia emission inventory with high-resolution and its evaluation in the Beijing–Tianjin–Hebei
724 (BTH) region, China, Atmospheric Environment, 106, 305-317,
725 <http://dx.doi.org/10.1016/j.atmosenv.2015.01.069>, 2015.
726



728
 729 **Fig. 1.** The satellite-derived observation numbers for NO₂ and NH₃. (a) denotes the percentages of observations in each month in
 730 2010 for NO₂ and in 2015 for NH₃ and (b) represents the total observation numbers for NO₂ and NH₃ over China. Notably, the
 731 NO₂ observation numbers were gained from DOMINO products with a cloud radiance fraction below 0.5, while the IASI
 732 observations with a relative error below 100% or an absolute error below 5×10^{15} molec. cm⁻² were processed for analysis over
 733 China.

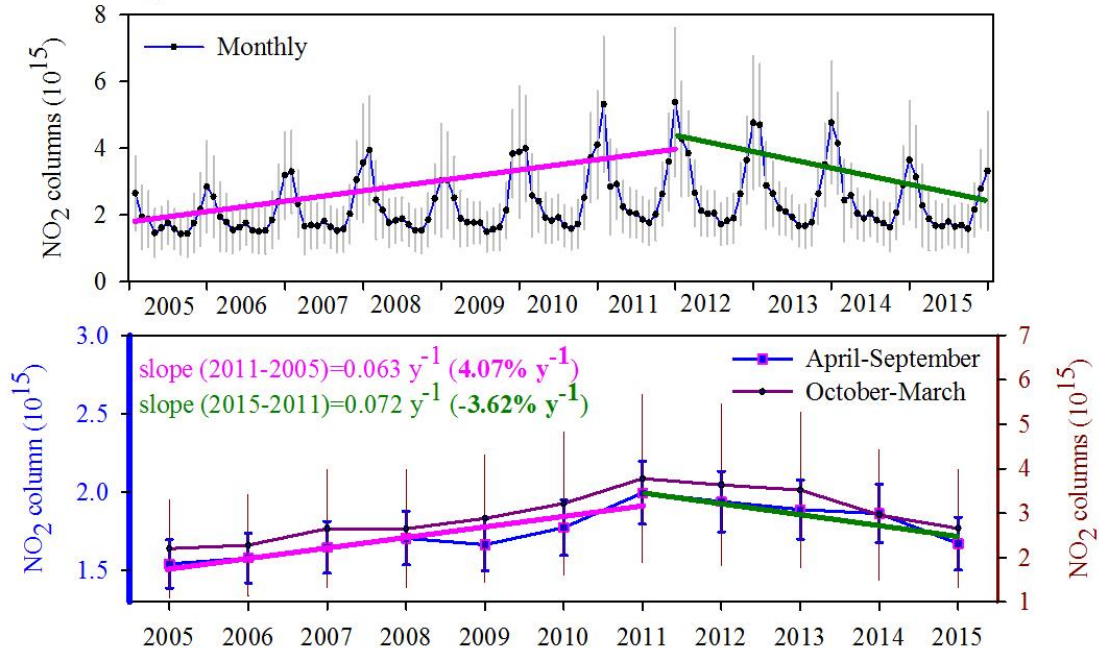


734

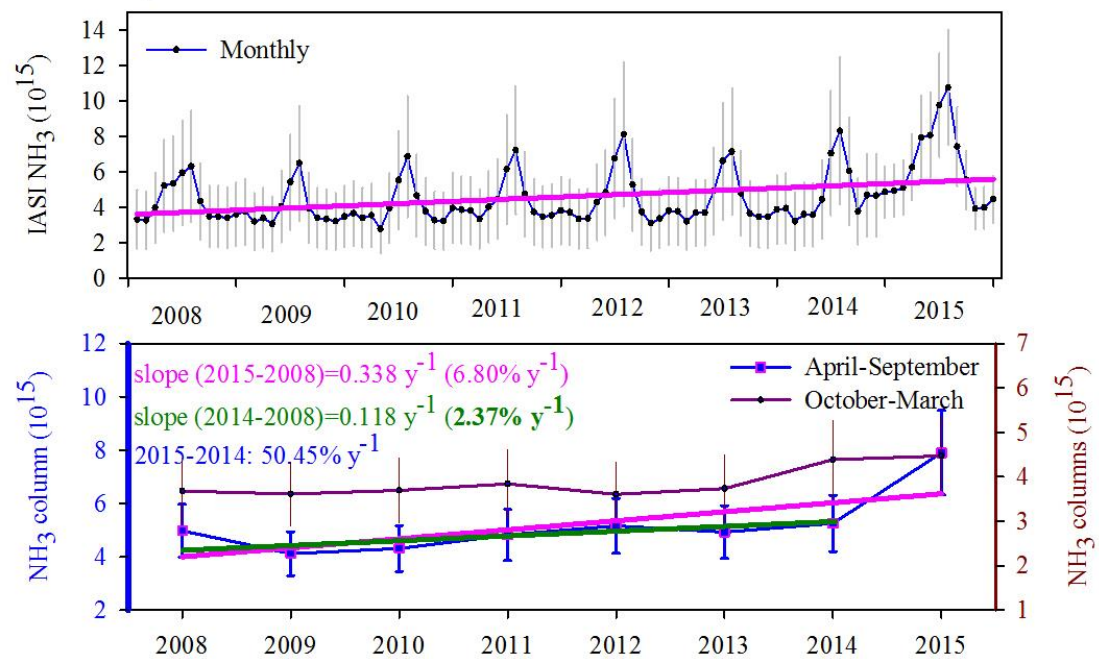
735 **Fig. 2.** The NO_2 and NH_3 emissions over China. (a) denotes the NO_2 and NH_3 emissions over China from 1980 to 2010 from
 736 REAS, (b) represents the NO_2 and NH_3 emissions over China from 1980 to 2010 from EDGAR, (c) demonstrates the relationship
 737 of NO_2 emissions over China from REAS and EDGAR and (d) shows the relationship of NH_3 emissions over China from REAS
 738 and EDGAR.

739

(a) OMI NO₂ at 13:45 P.M.



(b) IASI NH₃ at 9:30 A.M.



740

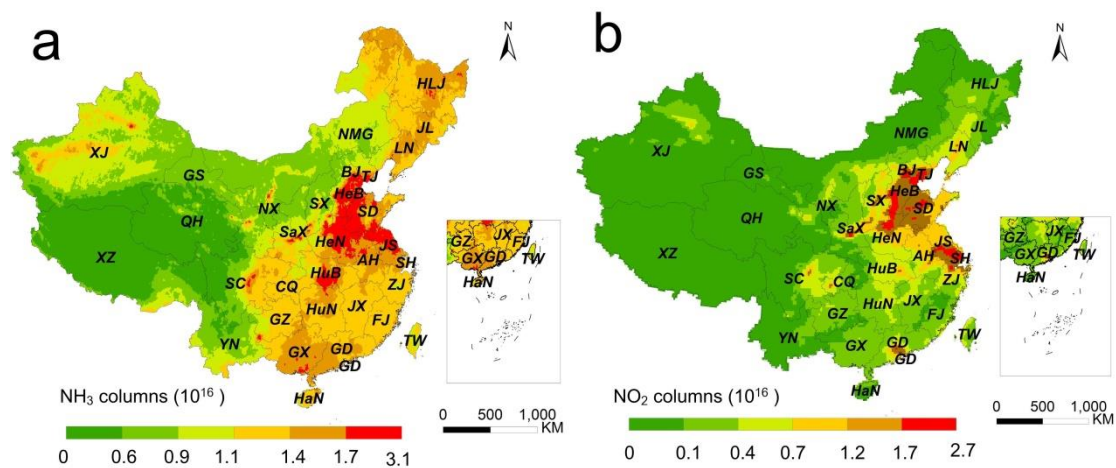
741 **Fig. 3.** Time series of average OMI NO₂ and IASI NH₃ columns over China during warm months (April-September) and cold

742 months (October-March). The time period of NO₂ columns was from 2005 to 2015, while the timespan of NH₃ columns was from

743 2008 to 2015 over China. The associated mean error for each period is presented here as error bars.

744

745



746

747

748

749

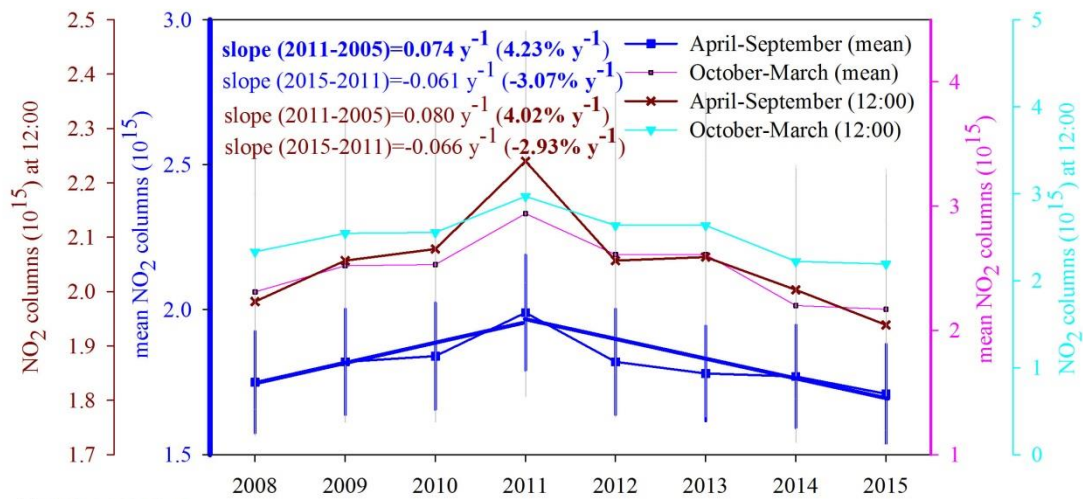
750

751

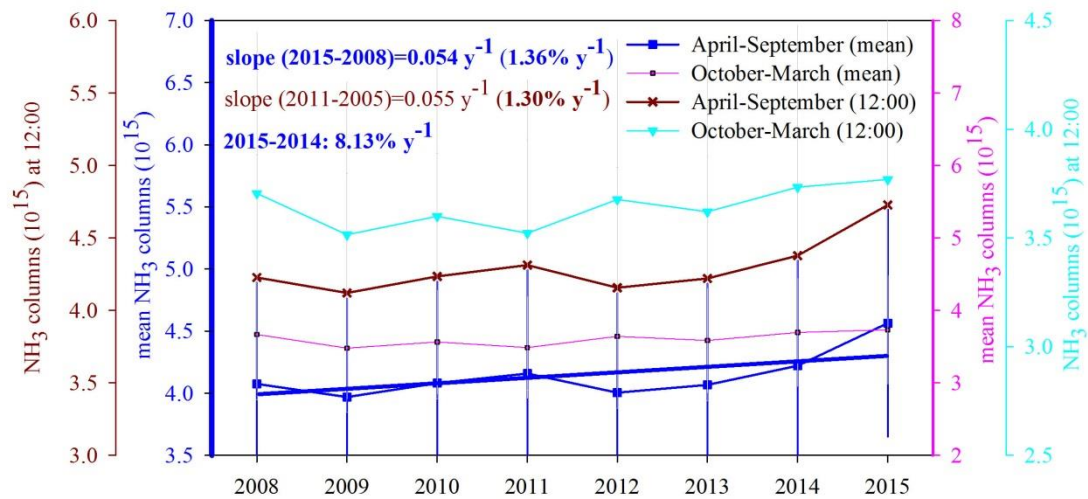
752

Fig. 4. Spatial distribution of the annual NH₃ (a) and NO₂ (b) columns (molecules cm⁻² year⁻¹). The successfully full provincial names are Beijing (BJ), Tianjin (TJ), Hebei (HeB), Shandong (SD), Shanxi (SX), Henan (HeN), Shaanxi (SaX), Liaoning (LN), Jilin (JL), Heilongjiang (HLJ), Neimenggu (NMG), Gansu (GS), Ningxia (NX), Xinjiang (XJ), Shanghai (SH), Jiangsu (JS), Zhejiang (ZJ), Anhui (AH), Hubei (HuB), Hunan (HuN), Jiangxi (JX), Fujian (FJ), Guangdong (GD), Hainan (HaN), Yunnan (YN), Guizhou (GZ), Chongqing (CQ), Sichuan (SC), Guangxi (GX), Xizang (XZ) and Qinghai (QH).

(a) MOZART NO₂



(b) MOZART NH₃



753

754

Fig. 5. Time series of MOZART NO₂ and NH₃ columns over China during average warm months (April-September) and cold months (October-March) from 2008 to 2015. The mean columns were calculated by averaging the columns at 00, 6, 12 and 18 h.

755

756

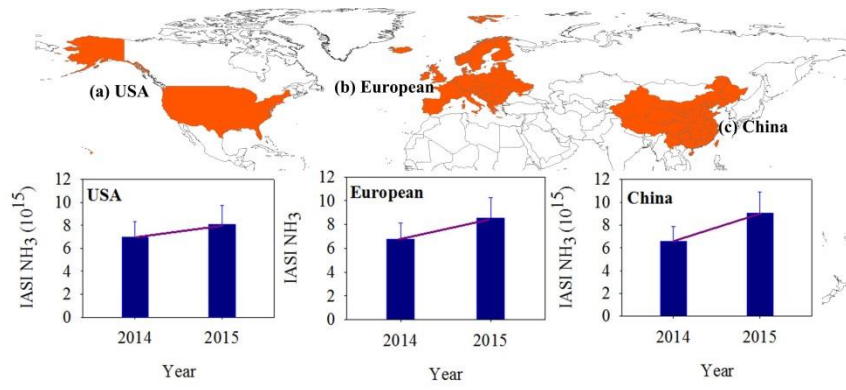
The associated mean error for each period is presented here as error bars.

757

758

759

760



761

762 **Fig. 6.** IASI NH₃ columns in USA, European and China between 2014 and 2015.

763